Application of a Three-Sensor Hot-Wire Probe for Incompressible Flow

T. L. Butler*
Pratt & Whitney Aircraft Group, East Hartford, Connecticut
and
J. W. Wagner†
United Technologies Research Center, East Hartford, Connecticut

An improved method for measuring velocity in three-dimensional, incompressible, turbulent flows using a three-sensor hot-wire or hot-film probe is presented. This technique determines the instantaneous velocity vector from three instantaneous senor outputs. A comparison of solutions from the new method to those from another method for a set of calibration data showed a considerable improvement in accuracy, angular resolution, and computation time. Also, intrastage measurements acquired from a large-scale axial flow research turbine were consistent with both theoretical predictions and measurements taken in similar flows using laser Doppler velocimetry. The good agreement with inviscid flow calculations and laser Doppler velocimetry measurements demonstrates that the new reduction method can be used to obtain accurate data for both mean and turbulent velocities in three-dimensional flows with high turbulence intensities.

Nomenclature

E_i	= output voltage from sensor i; i = A,B,C
EQ	= velocity parameter, $\sqrt{E_A^2+E_B^2+E_C^2}$
EP	= pitch angle parameter, $E_A/\sqrt{E_B^2+E_C^2}$
EY	= yaw angle parameter, E_B/E_C
iI,iJ,iK	= direction cosines for sensor i in X, Y, and Z directions; i = A,B,C
$\overline{q^2}$	= $\overline{u^2}+\overline{v^2}+\overline{w^2}$, turbulent kinetic energy
$\overline{u^2}, \overline{v^2}, \overline{w^2}$	= streamwise, normal, and radial components of Reynolds normal stress
$\overline{uv}, \overline{uw}, \overline{vw}$	= streamwise, normal, and radial components of Reynolds shear stress
Q_{eff_i}	= effective cooling velocity for sensor i; i = A,B,C
$\boldsymbol{Q}$	= velocity vector
Q	= velocity magnitude
θ_i	= sensor angle of i sensor; i = A,B,C
α	= pitch angle of velocity vector
β	= yaw angle of velocity vector
α_i	= pitch angle of sensor i; i = A,B,C
β_i	= yaw angle of sensor i; i = A,B,C

Introduction

At present, the most practical and widely used system for making velocity measurements in highly turbulent fluid flows is the hot-wire anemometer. Present hot-wire techniques have been refined to the point where fairly reliable measurements of mean and fluctuating velocities can be made in one- and two-dimensional flows where the mean flow direction is known and the turbulence intensity is less than approximately 10-15%. However, when the mean flow direction is unknown or the local turbulence intensities are high, these techniques can yield large errors for both mean and fluctuating velocities. Since there are many situations where both of these conditions exist, an improved measurement technique is essential to obtain accurate information about these flowfields.

Presented as Paper 82-0195 at the AIAA 20th Aerospace Sciences Meeting, Orlando, Fla., Jan. 11-14, 1982; submitted Jan. 22, 1982; revision received July 23, 1982.

*Senior Engineer, Commercial Engineering Division.
†Associate Research Engineer.

Over the past 10 years, various experimental investigators have attempted to use three-sensor probes to make velocity measurements in highly turbulent three-dimensional flows. A recent survey[1] has shown that many methods apply simplifying assumptions to reduce the complexity of the full hot-wire relationships which describe the response of sensors to changes in velocity magnitude and direction. However, these idealized relationships can lead to considerable errors in determining both mean and turbulent velocities when the flow is inclined at a nonoptimal angle relative to the probe. Other methods use more accurate response equations, but the numerical schemes necessary to solve these equations for the velocity vector make the processing of large amounts of data very costly.

In general, to reduce the measurement errors, the sensors must be calibrated over a wide range of velocity magnitudes and flow angles, and the resulting calibration data must be curve fitted in such a manner that the response of the sensors to changes in the velocity vector can be accurately represented. In addition, the curve fits to the calibration data should be in a form such that they can be solved for the velocity vector rapidly and efficiently.

This paper presents a new method for the calibration and use of a three-sensor hot-wire or hot-film probe which offers several advantages over existing methods. The method was developed to allow rapid, efficient processing of large amounts of data taken between stages in a large-scale, low-speed, experimental turbine.

New Method

With the new method, the probe is calibrated over a range of flow directions and velocity magnitudes representative of those expected to occur during actual data acquisition. The resulting calibration data are least square fitted to quadratic polynomials, which describe the response of the sensors to the velocity vector very accurately for a wide range of conditions.

Probe Description

The relationship between the velocity vector, an individual sensor, and the probe coordinate system is illustrated in Fig. 1. One of three sensors, i, is shown. Its spatial orientation is described by the unit vector

$$i = iTi + iJj + iKk \tag{1}$$

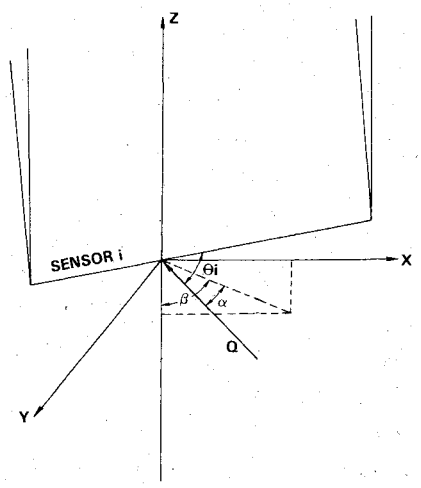

Fig. 1 Velocity vector and sensor geometry.

Here, i=A, B, or C denotes each of the three sensors. The velocity vector Q makes an angle θ_i with the i sensor. Both the sensor unit vector and the velocity vector can also be described by pitch and yaw angles, α and β, where α is the angle between the vector and its projection in the X-Z plane and β is the angle between the projection of the vector in the X-Z plane and the Z axis. The yaw and pitch angles of the velocity vector and sensor unit vectors are related to their respective components by the following equations:

$$Qy=-Q\sin\alpha, Qz=Q(\cos\alpha)(\cos\beta), Qx=Q(\cos\alpha)(\sin\beta) \quad (2)$$

$$iJ=\sin\alpha_i, \quad iK=(\cos\alpha_i)(\cos\beta_i, \quad iI=(\cos\alpha_i)(\sin\beta_i) \quad (3)$$

Expressions for the three sensor angles in terms of the yaw and pitch angles of velocity vector and the sensor unit vectors can be obtained by taking the dot product of the velocity vector with each of the three-sensor unit vectors,

$$\cos\theta_A = AI(\cos\alpha)(\sin\beta) - AJ(\sin\alpha) + AK(\cos\alpha)(\cos\beta)$$

$$\cos\theta_B = BI(\cos\alpha)(\sin\beta) - AJ(\sin\alpha) + BK(\cos\alpha)(\cos\beta)$$

$$\cos\theta_C = CI(\cos\alpha)(\sin\beta) - CJ(\sin\alpha) + CK(\cos\alpha)(\cos\beta) \quad (4)$$

Two standard "off-the-shelf" probes, each with different sensor orientations, were used during the test. A schematic of probe 1 is shown in Fig. 2, along with a summary of the sensor orientations for both probes. Sensor orientations were determined by using an optical telescope. All of the sensors were cylinderical hot films with length-to-diameter ratios of about 50. Both probes included a 0.5 mm (0.02 in.) diam thermocouple for correction of sensor outputs due to temperature variation from the calibration temperature. The large size of the probes relative to custom-designed subminiature probes was not felt to present a severe problem for this application because of the large size of the airfoils used in the experimental apparatus. However, a smaller subminature probe would give better spatial resolution and, in principle, could easily be used with this method. Figure 3 illustrates the contours of constant sensor angle θ_i as functions of the yaw and pitch angles of the velocity vector obtained from Eq. (4) for probe 1.

Probe Calibration

A fixed, low turbulence, constant velocity calibration jet was used for probe calibration. Linearizers were used to provide sensor output voltages that were linear with the approximate effective cooling velocity, resulting in the

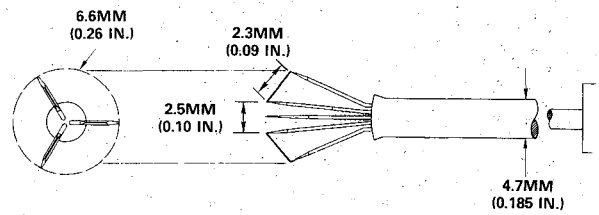

SENSOR ORIENTATIONS

PROBE	α_A	β_A	α_B	β_B	α_C	β_C
PROBE 1	-48.50	0.49°	19.1°	37.5°	16.5°	-38.5°
PROBE 2	-40.8	0°	0°	40.0°	0°	-40.0°

Fig. 2 Schematic of three-sensor probe.

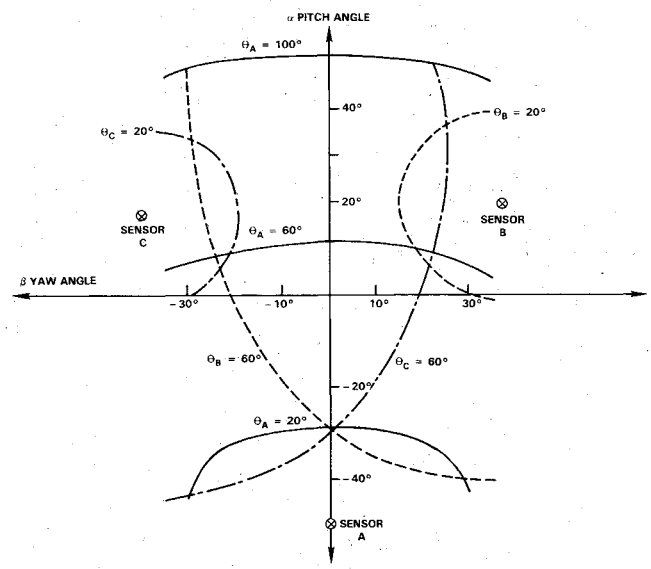

Fig. 3 Sensor angle contours for probe 1.

following relationship,

$$Q_{\text{eff}_i} = K_1 + K_2 E_i \quad (5)$$

The approximate effective cooling velocity was assumed to be equal to the total velocity when the sensor was oriented normal to the calibration jet. The coefficients K_1 and K_2 in Eq. (5) for each sensor were determined by varying the jet velocity with the sensor in this orientation. During testing, the linearized sensor outputs were corrected for flow temperature drift away from the calibration temperature by the following correction,

$$E_{i\text{corr}} = E_{i\text{meas}} \left(\frac{T_{\text{wire}} - T_{\text{cal}}}{T_{\text{wire}} - T_{\text{meas}}} \right)^2 \quad (6)$$

Here, T_{wire} is the film temperature [248°C (480°F) for this test], T_{cal} the flow temperature during calibration, and T_{meas} the flow temperature measured by the thermocouple.

Probe angular response was calibrated by varying the yaw and pitch angles of the probe with respect to the calibration jet. Yaw and pitch angles as well as the three linearized sensor voltages and velocity magnitude were recorded at each angular position. This procedure was repeated at several velocity levels. Calibration ranges used for the two probes are listed below.

Probe 1: $-35 \le \alpha \le 40$ deg, $-40 \le \beta \le 40$ deg

Probe 2: $-15 \le \alpha \le 15$ deg, $-20 \le \beta \le 20$ deg

In order to obtain accurate fits to the calibration data and to avoid iteration in the solution for the velocity vector, correlating parameters were chosen such that they gave a good collapse of the calibration data over a wide range of flow conditions and could be expressed in terms of the linearized sensor outputs. Several different correlating functions were tried. The best fits were obtained using the parameters and functional forms described below.

Because of the linear sensor output-effective velocity relationship, a representative velocity magnitude parameter was found to be,

$$EQ \equiv \sqrt{E_A 2 + E_B 2 + E_C 2} \tag{7}$$

The choice of representative pitch and yaw angle parameters depends on the orientation of the sensors relative to the probe coordinate system. For both probes used in this test, the following parameters provided good correlation,

$$EP \equiv E_A / \sqrt{E_B 2 + E_C 2}, \text{ pitch angle parameter} \tag{8}$$

$$EY \equiv E_B / E_C, \text{ yaw angle parameter} \tag{9}$$

The calibration data for velocity magnitude were fit according to the following quadratic relationship:

$$\begin{aligned} Q = {} & AQ_0 + (AQ_1)(EQ) + (AQ_2)(EQ)^2 + (AQ_3)(EP) \\ & + (AQ_4)(EP)^2 + (AQ_5)(EY) + (AQ_6)(EY)^2 \\ & + (AQ_7)(EQ)(EP) + (AQ_8)(EQ)(EY) \\ & + (AQ_9)(EP)(EY) \end{aligned} \tag{10}$$

Coefficients AQ_0 through AQ_9 were obtained by a least squares fit of the calibration data, a sample of which is plotted in Fig. 4. The fits were accurate to within $\pm 5\%$ for most of the data.

Calibration data for sensor angle were fitted in terms of velocity magnitude, effective velocity ratio, and voltage level parameters, as follows:

$$\begin{aligned} \theta_i = {} & TPi_0 + (TPi_1)(Q) + (TPi_2)(Q)^2 + (TPi_3)(Fi) \\ & + (TPi_4)(Fi)^2 + (TPi_5)(EP) + (TPi_6)(EP)^2 \\ & + (TPi_7)(EY) + (TPi_8)(EY)^2 + (TPi_9)(Q)(Fi) \\ & + (TPi_{10})(Q)(EP) + (TPi_{11})(Q)(EY) \\ & + (TPi_{12})(Fi)(EP) + (TPi_{13})(Fi)(EY) \\ & + (TPi_{14})(EP)(EY) \end{aligned} \tag{11}$$

where $i = \text{A, B, C}$ and $Fi = (Q_{\text{eff}}/Q)_i$.

Coefficients TPi_0 through TPi_{14} were also determined by least squares fitting. Data for one sensor on probe 1 are shown in Fig. 5. Also plotted is the classical cosine law. As shown, the parallel component of velocity contributes to the response of the sensor. Also note that sensor response is not rotationally symmetric; different values for Q_{eff}/Q occur at the same value of sensor angle. Equations (11) were found to be accurate within $\pm 5\%$ for most of the calibration data.

Figure 5 shows that sensor response is not linear with sensor angle. This implies that, in flows where the flow angle is changing greatly, averaging the sensor outputs and subsequently reducing the averaged sensor output to the velocity vector will not give a true indication of the flow angle. In flows of this nature, the simultaneously obtained instantaneous outputs must be reduced to an instantaneous velocity vector before averaging in order to obtain a measure of the true averaged flow angle. This method was used in the present study.

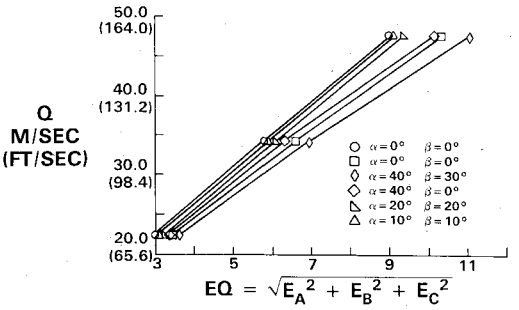

Fig. 4 Velocity magnitude calibration data.

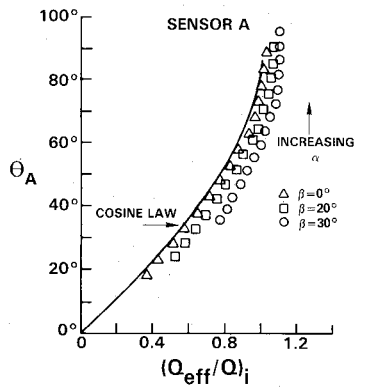

Fig. 5 Angular calibration data, 15.2 m/s (49.8 ft/s).

Reduction Method

Once the simultaneously obtained instantaneous sensor outputs have been obtained, the voltage level parameters are calculated and substituted into Eq. (10), which is then solved for instantaneous velocity magnitude. Equations (11) are then solved for the instantaneous values of θ_A, θ_B, and θ_C. From Fig. 3, it is evident that given values for any two sensor angles in the range $0 \le \theta_i \le 90$ deg there exist two possible solutions for α and β. In the Appendix a trigonometric solution is derived that relates θ_A and either θ_B or θ_C to α and β.

The accuracy of the method depends solely on the accuracy with which Eqs. (10) and (11) fit the calibration data. This accuracy decreases rapidly as sensor angles approach 0 and 90 deg. At these orientations, the fits for velocity magnitude and sensors angles, as described by Eqs. (10) and (11), have relatively large errors. In addition, at angles approaching 90 deg, the sensors become relatively insensitive to sensor angle and very sensitive to velocity magnitude. Thus, very accurate values of velocity magnitude are needed from Eq. (10) for substitution into Eq. (11) to obtain accurate solutions for sensor angle. By judicious choice of either the trigonometric solution using θ_A and θ_B with θ_C as a root check or the solution using θ_A and θ_C with θ_B as a root check (see Appendix), regions of undesirable sensor angle can be avoided. Using probe 1 as an example, it is evident from Fig. 3 that for $-25 \le \alpha \le 25$ deg and $\beta \ge 0$ deg, the θ_A or θ_B solution is the best choice because θ_C can approach 90 deg in this region. Similarly, for the region $-25 \le \alpha \le 25$ deg and $\beta \le 0$, the θ_A and θ_C solutions are the better choices because θ_B can approach 90 deg. In the region $\alpha > 25$ deg, the choice is not so clear-cut because θ_A approaches 90 deg and θ_B and θ_C can approach 0 deg. In this region, both solutions are done and then compared to discriminate unresolvable data.

Results

Calibration Data

To access the accuracy of this technique, the calibration data were reduced to velocity vectors by the new method and the solutions were compared to those obtained from Ref. 2. The method in Ref. 2 was originally intended to be used for our data reduction and it was designed for use with a single-

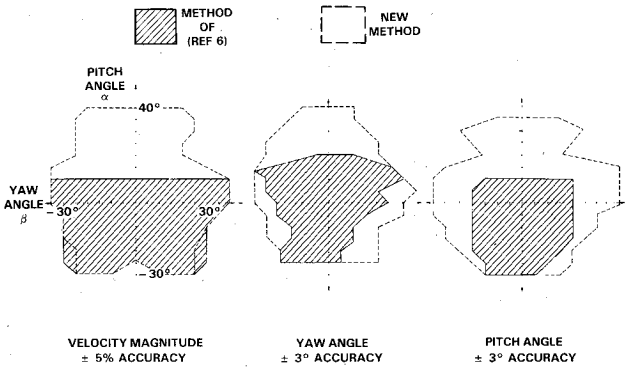

Fig. 6 Accuracy limits of solutions for calibration data, probe 1.

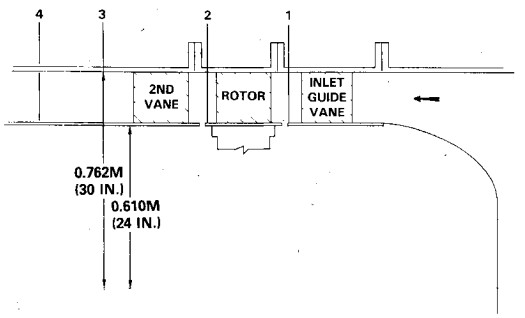

Fig. 7 United Technologies Research Center large-scale rotating research turbine.

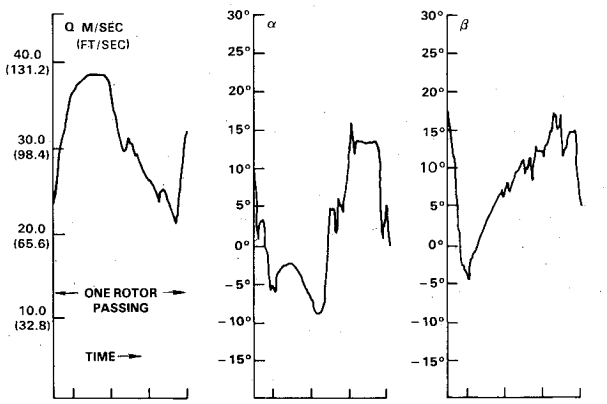

Fig. 8 Mean velocity measured at midspan downstream of rotor.

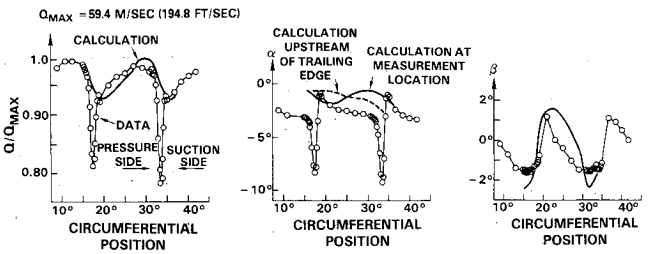

Fig. 9 Mean velocity measured at midspan downstream of inlet guide vane.

sensor probe rotated into multiple orientations. However, it can be applied to multiple-sensor probes. With slight modifications, the new method can also be used for single-sensor probes rotated into multiple orientations. Comparisons of the accuracy limits of the solutions of both methods for calibration data taken with probe 1 are shown in Fig. 6. As indicated, the range of incident yaw and pitch angles of the flow for which the velocity vector can be obtained accurately is greatly extended by the new method. Moreover, accuracy improves as the yaw and pitch angles of the incident flow approach 0 deg. Over the ranges of $-15 \leq \alpha \leq 15$ and $-20 \leq \beta \leq 20$ deg, the velocity magnitude can be determined within $\pm 1\%$ and the yaw and pitch angles of the velocity vector can be determined within ± 1 deg. In addition to improved angular resolution, the new method solves for the velocity vector in about one-fifth the time necessary for the method in Ref. 2. Since both techniques require the same type of probe calibration and analysis of calibration data, the new method allows for the processing of large amounts of data more quickly and inexpensively.

Unsteady Intrastage Turbine Measurements

The present method was developed to make measurements between stages in a large-scale, low-speed, axial flow research turbine. Figure 7 shows a schematic of the turbine and the measurement planes, while a description of the facility can be found in Ref. 3. The instantaneous sensor voltages were converted into an instantaneous velocity vector whose components were phase-lock ensemble averaged over 100 successive revolutions. A more complete description of the experimental program is contained in Ref. 4.

Figure 8 shows the phase-lock ensemble averaged velocity magnitude along with the flow yaw and pitch angles at the mean radius downstream of the rotor as a function of time as measured using probe 1 and the new data reduction technique.The probe was aligned at the meanline flow angle (40 deg from axial) such that deviations from this direction were measured as yaw angle (positive in rotor direction) and radial flows were measured as pitch angle (positive toward tip). In the midgap flow region, where the yaw and pitch angles are small, results from the method in Ref. 2 show good agreement with the new method. This is expected since the calibration data showed that both methods provide good accuracy when the flow is aligned with the probe. However, in the rotor wake, where the flow is misaligned with the probe, the two methods disagree. In this region, the method of Ref. 2 yields meaningless results because of the failure of the numerical technique to yield a converged solution.

The six components of Reynolds stress, in addition to mean velocity, were measured downstream of the inlet guide vane at the mean radius using probe 2 and the new reduction method. Turbulence quantities were obtained by combining the instantaneous velocity components with the phase-lock ensemble averaged velocity components and then phase-lock ensemble averaging again. Because of the large axial spacing between the guide vane and rotor, the flow was essentially steady at this location and the results have been time averaged over three rotor passings. The probe was aligned with the meanline flow angle (69 deg from axial).

Figure 9 shows the mean velocity and the yaw and pitch angles. It is instructive to note that the effective probe sensing diameter is approximately one-fifteenth of the wake width at this location. Also shown are predictions for the mean flow from the three-dimensional inviscid flow calculation of Ref. 5. Outside the wakes, the data and calculations for velocity mangitude and yaw angles agree very well, indicating that the measured variations accurately represent the inviscid flow effects. The disagreement between the measured and predicted pitch angles may be due to finite blockage present because of the wake velocity deficit (which is not accounted for in the calculation). This is supported by the fact that just upstream of the trailing edge, where the calculation accounts for a finite blockage, the agreement between the measurements and predictions is much improved.

The six components of Reynolds stress as well as the turbulent kinetic energy are shown in Fig. 10. Olson and Orloff[6] recently measured the Reynolds stress components in the wake of a two-dimensional NACA 4412 airfoil section using a laser Doppler anemometer (LDA). At one of their measurement locations, the ratio of the wake centerline

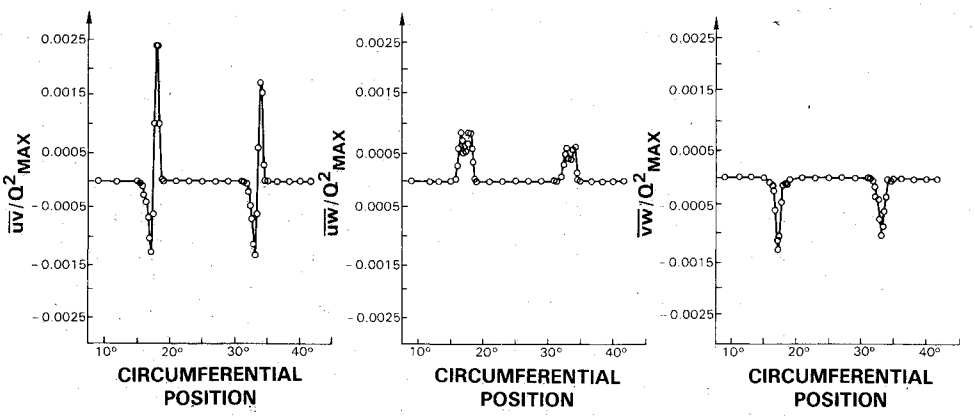

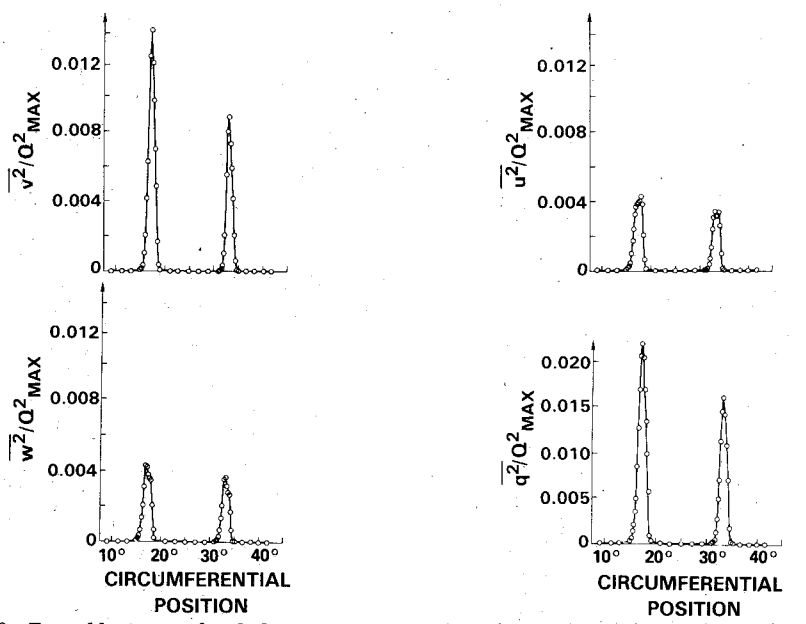

Fig. 10 Reynolds stress and turbulent energy measured at midspan downstream of inlet guide vane.

Table 1 Peak values of stress components of data

Reynolds stress components	Present method	LDV
$\overline{u^2}/Q^2_{max}$	0.0044	0.0047
$\overline{v^2}/Q^2_{max}$	0.0139	0.0073
$\overline{w^2}/Q^2_{max}$	0.0044	—
$\overline{uv}/Q^2_{max}$, suction side	0.0024	0.0026
$\overline{uv}/Q^2_{max}$, pressure side	0.0012	0.0015
$\overline{uw}/Q^2_{max}$	0.0008	—
$\overline{vw}/Q^2_{max}$	−0.0013	—

velocity to freestream velocity was approximately 80%. This corresponds closely with the centerline-freestream velocity ratio measured in the first wake of the present study. In both cases, the Reynolds numbers based on wake thickness and local freestream flow conditions were high enough to insure a fully turbulent flow. Thus, these two data sets afford a good comparison of Reynolds stresses measured by an LDA method and the new method for a partially mixed fully turbulent wake.

Table 1 lists the peak values of each of the stress components for both sets of data. Note that the peak value for the U component of normal stress is about the same in both cases. This is to be expected because the production of this component is proportional to the mean rate of strain $\partial U/\partial y$, which is similar in both cases. The peak value for the V component of normal stress is larger than the U component in both flows because of the absence of wall damping which tends to reduce the V component relative to the U component in boundary-layer flows. The agreement between the peak U component of shear stress ($\overline{uv}$) on both pressure and suction sides of the wake is also very good, as expected, because the generation of this component is also proportional to the mean strain rate $\partial U/\partial y$. The three-dimensional nature of the guide vane wake results in the extra rate of mean strain $\partial W/\partial y$ which is not present in the two-dimensional flow of Ref. 6. The additional rate of strain gives rise to the extra shear stress components ($\overline{uw}$) and ($\overline{vw}$) and may also be responsible for the larger V component of normal stress measured in the present study relative to that measured in Ref. 6. Also shown in Fig. 10 is the normalized turbulent kinetic energy. Note that in the center of the first wake the turbulence velocity is approximately 20% of the local mean velocity.

Conclusion

An improved method has been demonstrated for measuring velocity in three-dimensional incompressible turbulent flows using a three-sensor hot-wire probe. In comparison to present methods, this technique is considerably simpler, offers higher accuracy over a wide range of flow angles, and significantly reduces computing time. The method is particularly ap-

plicable to flows of unknown direction or high turbulence intensities where large quantities of data must be acquired. For such cases it offers improved accuracy in the measurement of mean and turbulent velocities at significantly reduced data processing costs.

Appendix: Determination of Yaw and Pitch Angles Directly from Sensor Angles

If the orientation of the velocity vector with respect to any two of the three sensors is known, then its orientation with respect to the probe coordinates (X-Y-Z coordinates) is limited to two possible directions. The orientation of the velocity vector with respect to the third sensor determines the correct direction. For illustrative purposes, sensors A and B will be used to derive the solution for the two possible velocity directions, although solutions can be derived using any two of the three sensors.

The velocity vector can be split into components perpendicular and parallel to the two sensors. Unit velocity vector perpendicular to sensor A:

$$Q_{NA} = Q_{NAX}i + Q_{NAY}j + Q_{NAZ}k \tag{A1}$$

Unit velocity vector perpendicular to sensor B:

$$Q_{NB} = Q_{NBX}i + Q_{NBY}j + Q_{NBZ}k \tag{A2}$$

Relationships between the direction cosines of the perpendicular and parallel components of the velocity vector to each sensor are obtained by setting the dot product of each of their respective unit vectors to zero.

$$Q_{NB} \cdot \mathrm{B} = 0$$

$$Q_{NBX}(\mathrm{B}I) + Q_{NBY}(\mathrm{B}J) + Q_{NBZ}(\mathrm{B}K) = 0 \tag{A3}$$

Similarly for sensor A:

$$Q_{NA} \cdot \mathrm{A} = 0$$

$$Q_{NAX}(\mathrm{A}I) + Q_{NAY}(\mathrm{A}J) + Q_{NAZ}(\mathrm{A}K) = 0 \tag{A4}$$

By equating the X-Y and Z components of velocity written in terms of the parallel and perpendicular components to each sensor, relstionships between the directions cosines of the perpendicular components can be obtained. For example, Qx can be written in tems of components perpendicular and parallel to sensor A as follows:

Qx = (X projection of velocity component parallel to sensor A) + (X projection of velocity component perpendicular to sensor A)

$$Qx = Q(\cos\theta_{\mathrm{A}})(\mathrm{A}I) + Q(\sin\theta_{\mathrm{A}})(Q_{NAX}) \tag{A5}$$

Qx can also be written in terms of components perpendicular and parallel to sensor B,

$$Qx = Q(\cos\theta_{\mathrm{B}})(\mathrm{B}I) + Q(\sin\theta_{\mathrm{B}})(Q_{NBX}) \tag{A6}$$

Combining Eqs. (A5) and (A6) gives:

$$Q_{NBX} = Q_{NAX}\left(\frac{\sin\theta_{\mathrm{A}}}{\sin\theta_{\mathrm{B}}}\right) + \frac{(\cos\theta_{\mathrm{A}})\mathrm{A}I - (\cos\theta_{\mathrm{B}})\mathrm{B}I}{\sin\theta_{\mathrm{B}}} \tag{A7}$$

Similar equations can be derived by equating the Y and Z components of velocity:

Y component

$$Q_{NBY} = Q_{NAY}\left(\frac{\sin\theta_{\mathrm{A}}}{\sin\theta_{\mathrm{B}}}\right) + \frac{(\cos\theta_{\mathrm{A}})\mathrm{A}J - (\cos\theta_{\mathrm{B}})\mathrm{B}J}{\sin\theta_{\mathrm{B}}} \tag{A8}$$

Z component

$$Q_{NBZ} = Q_{NAZ}\left(\frac{\sin\theta_{\mathrm{A}}}{\sin\theta_{\mathrm{B}}}\right) + \frac{(\cos\theta_{\mathrm{A}})\mathrm{A}K - (\cos\theta_{\mathrm{B}})\mathrm{B}K}{\sin\theta_{\mathrm{B}}} \tag{A9}$$

Equations (A3), (A4), and (A7-A9) represent a system of five linear simultaneous equations in the six unknowns: Q_{NAX}, Q_{NAY}, Q_{NAZ}, Q_{NBX}, Q_{NBY}, and Q_{NBZ}. This system, in general, has two solutions that correspond to the intersection of contours of constant sensor angle on the α-β plane as shown in Fig. 2. The solution of these five equations can be reduced to a simple quadratic equation for Q_{NAX} as follows.

Equations (A7-A9) can be substituted into Eq. (A3) to yield the following:

$$Q_{NAX}(\mathrm{B}I) + Q_{NAY}(\mathrm{B}J) + Q_{NAZ}(\mathrm{B}K) = -\left(\frac{(\mathrm{B}I)(FFI) + (\mathrm{B}J)(FFJ) + (\mathrm{B}K)(FFK)}{TR}\right) \tag{A10}$$

where

$$FFj \equiv \frac{\mathrm{A}j(\cos\theta\mathrm{A}) - \mathrm{B}j(\cos\theta\mathrm{B})}{\sin\theta_{\mathrm{B}}}, \quad j = I,J,K$$

$$TR \equiv \sin\theta_{\mathrm{A}}/\sin\theta_{\mathrm{B}}$$

When Eq. (A10) is solved for Q_{NAZ} and substituted into Eq. (A4) the following results:

$$Q_{NAX}(L) + Q_{NAY}(M) = N \tag{A11}$$

where:

$$L \equiv \frac{(\mathrm{B}K)(\mathrm{A}I)}{\mathrm{A}K} - \mathrm{B}I \qquad M \equiv \frac{(\mathrm{B}K)(\mathrm{A}J)}{\mathrm{A}K} - \mathrm{B}J$$

$$N \equiv \frac{(\mathrm{B}I)(FFI) + (\mathrm{B}J)(FFJ) + (\mathrm{B}K)(FFK)}{TR}$$

The definition of the unit vector gives

$$Q_{NAX}^2 + Q_{NAY}^2 + Q_{NAZ}^2 = 1 \tag{A12}$$

Combining Eqs. (A12) and (A4) results in:

$$Q_{NAX}\left(\frac{\mathrm{A}I}{\mathrm{A}K}\right) + Q_{NAY}\left(\frac{\mathrm{A}J}{\mathrm{A}K}\right) = \pm\sqrt{1 - Q_{NAX}^2 - Q_{NAY}^2} \tag{A13}$$

Equation (A11) can be substituted into Eq. (A13) to yield the following quadratic for Q_{NAX}:

$$Q_{NAX} = -W \pm \sqrt{W^2 - 4ZX}/2Z \tag{A14}$$

where:

$$W \equiv 2\left[\left(\frac{N}{M}\right)(\mathrm{A}I)(\mathrm{A}J) - \frac{NL}{M^2}(\mathrm{A}J^2 + \mathrm{A}K^2)\right]$$

$$X \equiv \left(\frac{N^2}{M^2}\right)(\mathrm{A}J^2 + \mathrm{A}K^2) - \mathrm{A}K^2$$

$$Z \equiv \left(\mathrm{A}I - \mathrm{A}J\frac{L}{M}\right)^2 + \mathrm{A}K^2\left(1 + \frac{L^2}{M^2}\right)$$

Once Q_{NAX} is known, Q_{NAY} is found from Eq. (A11) and then Q_{NAZ} can be found from Eq. (A4).

The equation for the Y component of velocity in terms of velocity components perpendicular and parallel to sensor A

which is similar to Eq. (A5) is

$$Q_y = Q(\cos\theta_A)(AJ) + Q(\sin\theta_A)(Q_{NAY}) \quad \text{(A15)}$$

This gives an equation for the pitch angle,

$$\alpha = \sin^{-1}[-AJ(\cos\theta_A) - Q_{NAY}(\sin\theta_A)] \quad \text{(A16)}$$

Similarly, an expression for the yaw angle can be obtained,

$$\beta = \sin^{-1}\frac{AI(\cos\theta_A) + Q_{NAX}(\sin\theta_A)}{\cos\alpha} \quad \text{(A17)}$$

As previously noted, Eq. (A14) implies two orientations for the velocity vector for known values of θ_A and θ_B. The unique solution for the direction of the velocity vector can be found by checking the value of the third sensor angle θ_C with the value of θ_C which occurs when the discriminant of Eq. (A14) vanishes. The discriminant of Eq. (A14) is zero when

$$W^2 = 4ZX \quad \text{(A18)}$$

This leads to an equation which gives the limiting value of θ_B, where a unique solution exists for any value of θ_A.

$$\cos(\theta_{Blim}) = (BIJKA)\cos\theta_A \pm \left(\frac{4(Z)(AK)}{LL^2 - 4Z\dfrac{AJ^2 + AK^2}{M^2}}\right)^{1/2}(\sin\theta_A) \quad \text{(A19)}$$

where $BIJKA \equiv (AI)(BI) + (AJ)(BJ) + (AK)(BK)$.

$$LL \equiv 2\left[\left(\frac{AIAJ}{M}\right) - \frac{L}{M^2}(AJ^2 + AK^2)\right]$$

The positive root of Eq. (A19) corresponds to solutions for θ_{Blim} and θ_A between 0 and 90 deg and is thus taken as the solution. These values are substituted into Eqs. (A16) and (A17) to obtain α_{lim} and β_{lim}. The value of θ_{Clim} is found from Eq. (4).

$$\cos\theta_C = CI(\cos\alpha)(\sin\beta) - CJ(\sin\alpha) + CK(\cos\alpha)(\cos\beta) \quad \text{(A20)}$$

θ_{Clim} is found from Eq. (A20) with α_{lim} and β_{lim}. The actual value of θ_C can be compared to θ_{Clim}. If θ_C is greater than θ_{Clim}, then the outer solution is correct and a plus sign is used in Eq. (A14). If θ_C is less than θ_{Clim} then the inner solution is correct and a minus sign is used in Eq. (A14).

Solutions that are analogous to the above method can be derived for any two of the three sensors.

References

[1] Butler, T. L. and Wagner, J. H., "An Improved Method for Calibration and Use of a Three Sensor Hot Wire Probe in Turbomachinery Flows," AIAA Paper 82-0195, 1982.

[2] Schmidt, D. P. and Okishi, T. H., "Multistage Axial Flow Turbomachine Wake Production, Transport and Interaction," Iowa State University, Engineering Research Institute, Ames Rept. 77130, Nov. 1976.

[3] Dring, R. P. and Joslyn, H. D., "Measurements of Turbine Rotor Blade Flows," *Journal of Engineering for Power*, Vol. 103, April 1981, pp. 400-405.

[4] Joslyn, H. D., Sharma, O. P., and Dring, R. P., "Unsteady Three-Dimensional Turbine Aerodynamics," ASME Paper GT-82-161, 1982.

[5] Denton, J. D., "A Time Marching Method for Two and Three-Dimensional Blade to Blade Flows," Aeronautical Research Council, R&M 3775, 1975.

[6] Olson, L. E. and Orloff, K. L., "On the Structure of Turbulent Wakes and Merging Shear Layers of Multielement Airfoils," AIAA Paper 81-1238, 1981.